© 1985 IEEE. Personal use of this material is permitted. However, permission to reprint/republish this material for advertising or promotional purposes or for creating new collective works for resale or redistribution to servers or lists, or to reuse any copyrighted component of this work in other works must be obtained from the IEEE.

IEEE Transactions on Nuclear Science, Vol. NS-32, No. 5, October 1985

NUMERICAL SIMULATION OF AN ACCELERATOR INJECTOR*

J. K. Boyd, G. J. Caporaso, A. G. Cole
Lawrence Livermore National Laboratory
P.O. Box 808
Livermore, California 94550

Abstract

Accelerator injector designs have been evaluated using two computer codes. The first code self consistently follows relativistic particles in two dimensions. Fields are obtained in the Darwin model which includes inductive effects. This code is used to study cathode emission and acceleration to full injector voltage. The second code transports a fixed segment of a beam along the remainder of the beam line. Using these two codes the effects of electrode configuration on emittance, beam quality and beam transport have been studied.

Introduction

Many anticipated experiments place constraints on acceptable beam emittance and quality. To study the effect of various accelerator injector designs on these parameters an effort is underway to numerically model the injector and subsequent transport. Generally, an accelerator injector design may be studied using either steady-state or time-dependent computer codes. The steady-state codes generally fix electrode voltages and then follow macro-particles or trace single particle rays until a solution is reached. Time-dependent codes are typically particle-in-cell (PIC) simulations. The PIC codes have a time step limitation and also tend to radiate anomalously large amounts of energy into electromagnetic modes.

In this work the problems of a full PIC electromagnetic simulation are avoided by using the Darwin field approximation [1-2]. This model has been implemented in the DPC (Darwin Particle Code) computer code. The Darwin model is the magnetoinductive limit of Maxwell's equations, which retains the first order relativistic correction to the particle Lagrangian. In the Darwin approximation inductive effects are modeled without creating non-physical radiation. The DPC code is consequently viewed as a useful implementation of a physics model which includes inductive effects absent from a steady state calculation.

The DPC code solves for the transport of a beam from emission through acceleration up to full energy. Subsequent transport is obtained from the WTC (Wire Transport Code) computer code [3]. The WTC code was originally written to study transport in the presence of an electrostatically charged wire. It has since been modified to additionally handle general transport through magnet elements and accelerating gaps.

Injector Evaluation Strategy

The desirability of an injector design is influenced by the requirement of matching into the rest of the accelerator. Consequently, injector designs are evaluated in two parts. First, the DPC code solves for beam dynamics over a distance of typically 50 cm. This includes the field emission from a cathode and acceleration up to the energy of the injector. Particle trajectories are followed from the emitting surface and past all electrodes including the anode. At this point beam transport is continued by using WTC to follow the motion of a group of particles which exit the DPC computational region during a time step. This amounts to following a slice of the beam at a fixed distance from the beam head. The DPC calculation reveals the immediate effect of parameter choices such as the A-K gap accelerating stress, electrode configuration and axial magnetic field profile. The WTC results show how a particular beam evolves into the accelerator including possible current loss and emittance growth.

*Performed jointly under the auspices of the U.S. DOE by LLNL under W-7405-ENG-48 and for the DOD under DARPA, ARPA Order No. 4395, monitored by NSWC.

DPC Model

DPC solves the relativistic force equation in cartesian x, y, z coordinates,

$$m \frac{d\vec{u}}{dt} = \frac{q}{c} \vec{E} + \frac{q}{c\gamma} \vec{u} \times \vec{B} \quad , \tag{1}$$

where m is particle mass, $\gamma = (1 - (v/c)^2)^{-1/2}$, v is velocity q is charge, c is the speed of light, $\vec{u} = \gamma\vec{v}/c$, $\vec{E}$ is the electric field and $\vec{B}$ is the magnetic field. Axisymmetry is assumed so fields are only functions of r and z. Consistent with this assumption the current and charge density are obtained from the particles by spreading these quantities in theta.

Fields are obtained from Maxwell's equations in the Darwin approximation. The practical consequence of the Darwin approximation is the neglect of the solenoidal part of the displacement current. Denoting solenoidal by subscript t and irrotational by subscript ℓ Maxwell's equations in the Darwin approximation are below.

$$\nabla \cdot \vec{B}_t = 0 \tag{2a}$$

$$\nabla \times \vec{B}_t = \frac{4\pi}{c} \vec{J} + \frac{1}{c} \frac{\partial \vec{E}_\ell}{\partial t} \tag{2b}$$

$$\nabla \cdot \vec{E}_\ell = 4\pi\rho \tag{2c}$$

$$\nabla \times \vec{E}_t = -\frac{1}{c} \frac{\partial \vec{B}_t}{\partial t} \quad . \tag{2d}$$

Hereafter $\vec{B}_t$ will be denoted by $\vec{B}$ since a magnetic field is strictly solenoidal.

DPC solves for fields on a rectangular r, z grid which contains an anode, a cathode and may also contain additional electrodes. Since axisymmetry is assumed it is not necessary to obtain the solenoidal part of the source terms to solve Eq. (2b). In the most general Darwin model because the left side of Eq. (2b) is solenoidal this step is necessary. In the DPC implementation the following two elliptic equations are solved for B,†

$$\Delta^* \psi_A = -4\pi \, r \, J_{\theta/c} \tag{3a}$$

$$\Delta^* \psi_B = \frac{4\pi}{c} r \left(\frac{\partial J_z}{\partial r} - \frac{\partial J_r}{\partial z} \right) \quad , \tag{3b}$$

where $\psi_B = rB_\theta$, $\psi_A = rA_\theta$ and A_θ is the theta component of the vector potential. Solving for ψ_B gives B_θ and the other two components are,

$$B_r = -\frac{1}{r} \frac{\partial \psi_A}{\partial z} \quad , \quad B_z = \frac{1}{r} \frac{\partial \psi_A}{\partial r} \quad . \tag{4}$$

0018-9499/85/1000-2602$01.00© 1985 IEEE

The DPC electric field is calculated from equations obtained by letting $\vec{E}_\ell = -\nabla\phi$ in Eq. (2c) and taking the curl of Eq. (2d).

$$\nabla^2\phi = -4\pi\rho \tag{5a}$$

$$\nabla^2\vec{E}_t = \frac{4\pi}{c^2}\left(\frac{\partial\vec{J}}{\partial t}\right)_t \tag{5b}$$

WTC Model

WTC is a particle code [3] which transports a group of particles exiting the DPC computational domain in one time step. This relativistic beam slice is transported in the paraxial approximation with the z velocity assumed to be the speed of light for all particles. Thus, z = ct and only the transverse trajectory is calculated from the following force equations.

$$\frac{\partial^2 x}{\partial z^2} = -\frac{c\,E_x}{\beta I_A} - \frac{c\,B_z}{I_A}\frac{\partial y}{\partial z} + \frac{c\,B_y}{I_A} \tag{6a}$$

$$\frac{\partial^2 y}{\partial z^2} = -\frac{c\,E_y}{\beta I_A} - \frac{c\,B_x}{I_A} + \frac{c\,B_z}{I_A}\frac{\partial x}{\partial z} \quad . \tag{6b}$$

The electric fields are obtained from the electrostatic equation.

$$E_r = \frac{4\pi}{r}\int_0^r \rho\, r\, dr \quad . \tag{7}$$

In Eq. (6) there is no E_θ contribution since inductive effects due to particle motion are not included. The magnetic field in Eq. (6) is due to the B_θ of the beam and magnetic fields of focus coils. The beam B_θ is obtained from Amperes law without a displacement current,

$$B_\theta = \frac{2\,I_r}{rc} \quad , \tag{8}$$

where I_r is the current enclosed at radius r. The magnetic field due to external coils is calculated from analytic formulas for the B_z (r,z) component. The B_r component is given by a rearrangement and integration of $\nabla \cdot \vec{B} = 0$.

$$B_r = -\frac{1}{r}\int_0^r \frac{\partial B_z}{\partial z}\, r\, dr \quad . \tag{9}$$

For large aspect ratio solenoids B_z is assumed to be independent of radius.

Results

Many different injector designs have been evaluated using a variety of diagnostics. The parameters for a typical diode configuration are given in Table 1.

Table 1

Peake voltage	2.4 MeV
Voltage rise time	20 ns
A-K gap	13 cm
Cathode radius	7 cm
Peak B_z	510 gauss

For this case DPC solves for beam dynamics in a region 16 cm in radius and 60 cm in the axial or z direction. Figure 1 illustrates the geometry showing the 8 cm anode bore which expands to 12.5 cm at z = 30 cm.

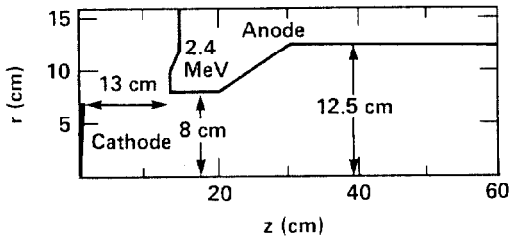

Figure 1. Geometry.

The electron beam produced by the accelerator must be born in a region free of magnetic field. A magnetic field on the cathode gives rise to an equivalent emittance contribution which is undesirable. Since a finite magnetic field is necessary to focus a beam expanding due to its space charge, the magnetic field increases from zero at the cathode. Figure 2 shows the $B_z(z)$ profile due to external coils.

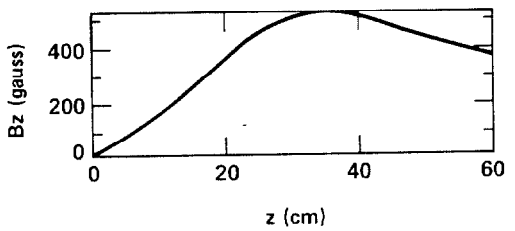

Figure 2. Magnetic field profile.

The peak B_z in Table 1 refers to the first maximum along the beam line which is shown in Fig. 2 at z = 35 cm. The magnetic field profile due to external coils is dc and thus it must be set for a beam at the full voltage.

DPC ran for a total of 30 ns which includes the 20 ns voltage rise time and 10 ns of steady state operation. During the rise time the effect of the energy mismatched dc magnetic field is clearly visible in the particle trajectories. At 5 ns intervals the DPC simulation was halted and test particles were launched at r = 2 cm from the cathode. The radius as a function of z is shown in Fig. 3 at t = 0, 5, 10, 15 ns respectively.

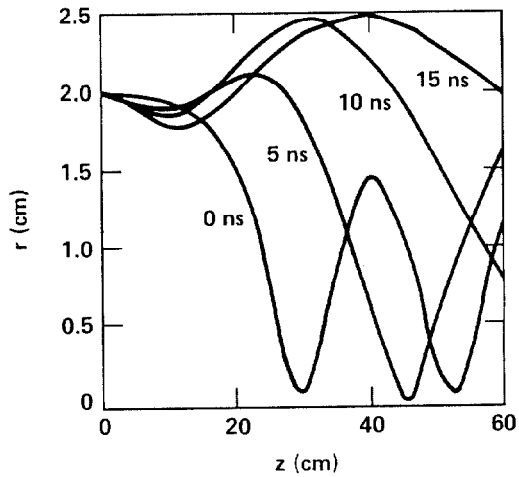

Figure 3. Particle trajectories, r(z).

The trajectory on the r, z plot is a projection showing an oscillation of increasing period as

time increases. This corresponds to higher energy as trajectories are followed further into the rise time.The actual trajectory is a helix. This can be verified by comparing the x, y orbit projection at t = 0 and 10 ns shown in Fig. 4.

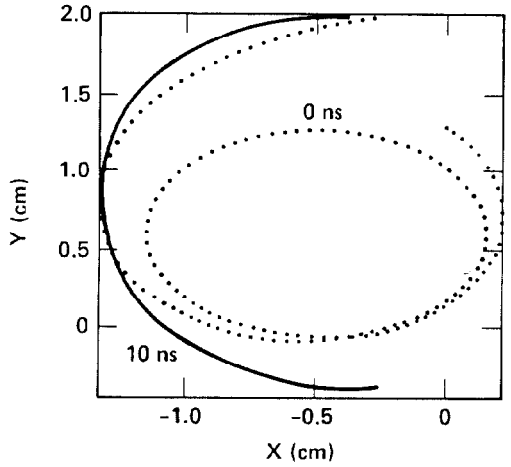

Figure 4. Particle trajectories, x, y.

The dotted trajectory at t = 0 spirals around almost an angle of 4π, whereas the solid trajectory rotates only π. The dc magnetic field is set for the highest energy or equivalently the "test" trajectories at the latest time. Thus, the t = 10 trajectory in Fig. 4 most closely characterizes a beam trajectory corresponding to the dc field. The orbit type (for this initial condition) changes from non-axis encircling to nearly axis encircling between t = 0 and t = 10.

One of the most useful diagnostics generated by DPC is the brightness $\mathcal{J}$, plotted as a function of current. In Eq. (10) I_z is the z directed current

$$\mathcal{J} = \pi^2 \, I_z/(\gamma^2\beta^2 V_4) \quad . \qquad (10)$$

enclosed by the V_4 phase space $(x,y,v_x/c,v_y/c)$ ellipsoid volume. Figure 5 shows $\mathcal{J}$ for particles with 57 cm < z < 60 cm and I_z ranging from 500 to 9100 amps. For this case $\mathcal{J}$ varies from 2×10^3 to 3.5×10^3 amp/(rad^2 - cm^2). The trough in the

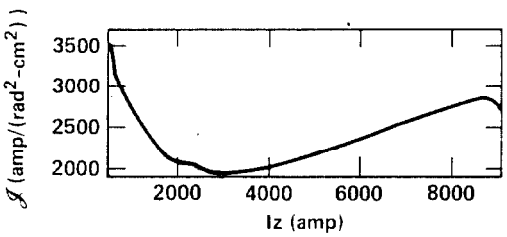

Figure 5. Brightness versus enclosed current.

curve near I_z = 3000 is indicative of diminished phase space current density in this region. Between 4000 and 8500 amps $\mathcal{J}$ is increasing which means the enclosed current increases more rapidly than V_4 over the corresponding region of phase space.

For this case the phase space exiting DPC at t = 30 ns has been transported 220 cm with the WTC code. The root mean square radius R(z) is plotted in Fig. 6. The z = 0 position corresponds to z = 60 on the DPC grid. The rectangles along the abscissa indicate the positions of magnet elements. It can be seen R decreases from 7.5 to 3.5 cm which focuses the beam into the 7 cm radius beam pipe. The oscillation wavelength is approximately 100 cm.

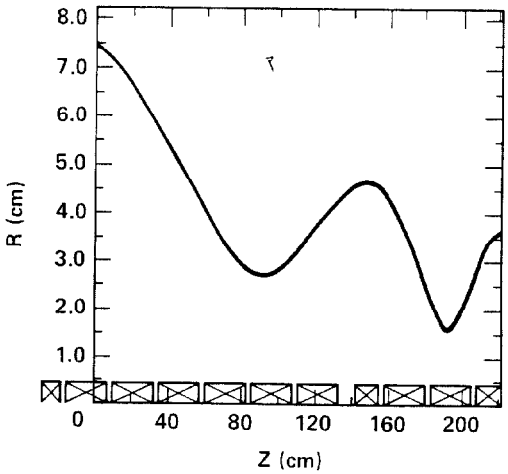

Figure 6. Beam radius versus z.

The behavior of $\mathcal{J}$ during transport is indicated by the inverse square of the normalized emittance, E plotted in Fig. 7. For uniformly filled phase space V_4 is proportional to E^2. In this case no current is lost so $\mathcal{J}$ is proportional to E^{-2}, assuming uniformly filled phase space. Within this approximation Fig. 7 shows $\mathcal{J}$ only has a 20% variation over 220 cm.

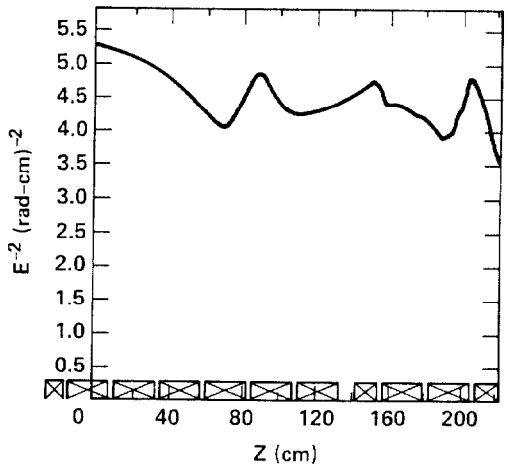

Figure 7. Inverse emittance squared.

References

[1] C. W. Nielson, H. R. Lewis, Methods in Computational Physics Vol. 16, p. 367 Academic Press, N.Y. 1976.

[2] D. W. Hewett, C. W. Nielson, J. Comp. Phys. 29 219 (1978).

[3] G. J. Caporaso, A. G. Cole, IEEE Trans. Nuc. Sci. Vol. NS-30, No. 4, p. 2618, Aug. 1983.

Acknowledgements

Gratitude is expressed for useful discussions with Drs. V. K. Neil, A. C. Paul, D. W. Hewett and S. S. Yu.

$^{\dagger}\Delta^* \equiv r^2 \, \nabla \cdot (r^{-2}\nabla$